THESIS FOR THE DEGREE OF DOCTOR OF PHILOSOPHY IN SOLID AND STRUCTURAL MECHANICS

# Long-term rail damage evolution in railway crossings

ROSTYSLAV SKRYPNYK

Department of Mechanics and Maritime Sciences

Division of Dynamics

CHALMERS UNIVERSITY OF TECHNOLOGY

Gothenburg, Sweden 2020

Long-term rail damage evolution in railway crossings
ROSTYSLAV SKRYPNYK
ISBN 978-91-7905-308-6



Doktorsavhandlingar vid Chalmers tekniska högskola
Ny serie nr. 4775
ISSN 0346-718X
Department of Mechanics and Maritime Sciences
Division of Dynamics
Chalmers University of Technology
SE-412 96 Gothenburg
Sweden
Telephone: +46 (0)31-772 1000

Cover:
Railway crossing at Norra Skara in Sweden. Photo by Albin Berlin, Pexels.

Chalmers Reproservice
Gothenburg, Sweden 2020

Long-term rail damage evolution in railway crossings
ROSTYSLAV SKRYPNYK
Department of Mechanics and Maritime Sciences
Division of Dynamics
Chalmers University of Technology

# Abstract

To accommodate the passage of wheels in intersecting traffic routes, fixed railway crossings have discontinuous rails leading to an intense load environment due to repeated wheel–rail impacts. This gives rise to high costs associated with repair and maintenance of the rails in the crossing. For given traffic conditions, several approaches to crossing design can be undertaken to mitigate the material degradation and hence reduce the life cycle cost. In the present thesis, the option of selecting a more suitable crossing material is explored.

To obtain a guideline for material selection, the in-track performance of different materials during the life of a crossing needs to be predicted. In this work, an existing simulation methodology is extended by improving its robustness and computational efficiency. The methodology is able to account for the dynamic vehicle–track interaction, resolve the elasto-plastic wheel–rail contact, and consider the main damage mechanisms related to the running surface of a crossing rail. In this thesis, the methodology is updated by including a metamodel of plastic wheel–rail normal contact, which is introduced to meet the computational challenge of performing a large number of finite element simulations. The metamodel is based on the contact theory of Hertz. It is shown that the metamodel yields accurate results while accounting for the inelastic material behaviour.

The simulation methodology is applied to several test cases. In the first study, it is employed to compare the short-term performance of two rail steel grades that are commonly used in crossings: the fine-pearlitic steel R350HT and the austenitic manganese steel Mn13. A representative load sequence generated by means of Latin hypercube sampling, taking into account variations in worn wheel profile, vehicle speed and wheel–rail friction coefficient, is considered. After 0.8 million gross tonnes (MGT) of traffic, it is predicted that the use of rolled Mn13 will result in approximately two times larger ratchetting strain as compared to the R350HT. In the second study, the methodology is used to simulate approximately 12 MGT of traffic in a crossing. The results of the simulations are compared with data measured in the field. It is shown that the simulations are in good qualitative agreement with the measurements. Finally, the methodology is used to quantify the difference in long-term damage between crossings with different crossing angles. As expected, the crossing with the largest crossing angle is subjected to the highest impact loads and exhibits the most damage after 52 MGT of simulated traffic.

Keywords: Dynamic vehicle–track interaction, switches & crossings, S&C, FEM, metamodel, wheel–rail contact mechanics, plasticity, wear

*To Proteus*

Anthropos apteros, perplexed
To know which turning to take next,
Looked up and wished he were the bird
To whom such doubts must seem absurd.

---

*Labyrinth*
Wystan Hugh Auden

# Preface

The work in this thesis has been carried out at the Department of Mechanics and Maritime Sciences at Chalmers University of Technology from May 2015 to May 2020 within the research project TS17 "Optimization of materials in track switches". This project is part of the research activities within the Centre of Excellence Chalmers Railway Mechanics (CHARMEC). The research has been funded within CHARMEC with special support from the Swedish Transport Administration (Trafikverket) and voestalpine VAE GmbH. Part of the funding was provided by the European Horizon 2020 Joint Technology Initiative Shift2Rail through projects In2Track (contract no. 730841) and In2Track-2 (contract no. 826255). The simulations were performed on resources at Chalmers Centre for Computational Science and Engineering (C3SE) provided by the Swedish National Infrastructure for Computing (SNIC).

# Acknowledgements

First of all, I would like to thank my supervisors: Professor Jens Nielsen, who, though not permanently located at Chalmers, always provided the needed assistance and gave me the most detailed feedback; Professor Magnus Ekh, who, due to his deep knowledge and vicinity of the office, probably suffered the most from my questions; Dr. Björn Pålsson, who is well known for his expertise in switches and crossings and with whom collaboration is a delight; and last but not least, Dr. Jim Brouzoulis, who, despite having left the project, still feels like part of the team.

Second of all, I would like to thank our industrial partners, and in particular, Mr. Uwe Ossberger and Mr. Heinz Ossberger of voestalpine VAE for initiating the project, providing measurement data and all the fruitful discussions we have had over these years.

Third of all, I would like to express my gratitude to friends and colleagues at the divisions of Dynamics and Material & Computational Mechanics for creating a nurturing environment. Special thanks to those of you also sharing your leisure time with me. I truly appreciate your friendship.

Finally, I want to extend my gratitude to my parents Elena and Alexander who always encouraged my interest in learning, and to my life partner Panagiota who helped me find equilibrium in life. Thank you for the love and support you surround me with!

Gothenburg, May 2020

Rostyslav Skrypnyk

# Thesis

This thesis consists of an extended summary and the following appended papers:

**Paper A** Skrypnyk, R., Nielsen, J. C. O., Ekh, M., Pålsson, B. A. (2019). Metamodelling of wheel–rail normal contact in railway crossings with elasto-plastic material behaviour. *Engineering with Computers* **35** (1), 135–155.

**Paper B** Skrypnyk, R., Ekh, M., Nielsen, J. C. O., Pålsson, B. A. (2019). Prediction of plastic deformation and wear in railway crossings – Comparing the performance of two rail steel grades. *Wear* **428-429**, 302–314.

**Paper C** Skrypnyk, R., Ossberger, U., Pålsson, B. A., Ekh, M., Nielsen, J. C. O. (2020). Long-term rail profile damage in a railway crossing: Field measurements and numerical simulations. *Accepted for publication in Wear.*

**Paper D** Skrypnyk, R., Pålsson, B. A., Nielsen, J. C. O., Ekh, M. (2020). Influence of crossing angle on long-term damage evolution in railway crossings. *To be submitted for international publication.*

The appended papers were prepared in collaboration with the co-authors. The author of this thesis was responsible for the major progress of the work, i.e. took part in planning of the papers and development of the theory, carried out numerical implementation and simulations, and prepared the manuscript.

Other related publications by the author not included in this thesis:

- Skrypnyk, R., Pålsson, B. A., Nielsen, J. C. O., Ekh, M. (2018). Metamodel for elasto-plastic wheel–rail contact with application to damage in a railway crossing. *Proceedings of the 25th International Symposium on Dynamics of Vehicles on Roads and Tracks, IAVSD 2017, August 14-18, 2017, Rockhampton, Australia.* Taylor & Francis Group, 705–710.
- Skrypnyk, R., Ekh, M., Nielsen, J. C. O., Pålsson, B. A. (2018). Simulation of damage in railway crossings – A comparison of rail steel grades R350HT and rolled Mn13. *Proceedings of the 11th International Conference on Contact Mechanics and Wear of Rail/Wheel Systems, CM 2018, September 24-27, 2018, Delft, The Netherlands.* TU Delft, 902–907.
- Skrypnyk, R., Nielsen, J. C. O., Pålsson, B. A., Ekh, M. (2020). Prediction of long-term damage in railway crossings accounting for variability in dynamic traffic loads. *Advances in Dynamics of Vehicles on Roads and Tracks: Proceedings of the 26th Symposium of the International Association of Vehicle System Dynamics, IAVSD 2019, August 12-16, 2019, Gothenburg, Sweden.* Ed. by M. Klomp et al. Springer International Publishing, 376–381.

# Contents

# Part I
# Extended Summary

## 1 Introduction

### 1.1 Background and motivation

To meet current and future challenges for the transport sector such as oil scarcity, growing populations and the need to reduce greenhouse emissions, the European Commission published a vision for the future European transport sector in a white paper in 2011 (EC 2011). According to this vision, transport will have to reduce greenhouse emissions by 60% below 1990 levels in order to meet the goal of 80-95% reduction for the entire economy by 2050. To this end, it was decided that at least 50% of road freight over medium distance (300 km) has to shift to rail or waterborne transport, and that the European high-speed rail network needs to be completed to facilitate for the majority of medium-distance passenger transport to go by rail. These measures imply an expansion of the European railway network and a sustained interest in cost effective railway solutions.

The railway turnout (switch and crossing, S&C) is an integral component of any rail network. It provides flexibility to the system by connecting different tracks. A top view of a turnout with its major components is depicted in Figure 1.1. The two main parts of a turnout, the switch panel and the crossing panel, give the turnout its alternative name and abbreviation. A more diligent account of S&C components, together with their taxonomy, can be found in Zwanenburg 2009. Vertical impact loads are induced in the crossing panel

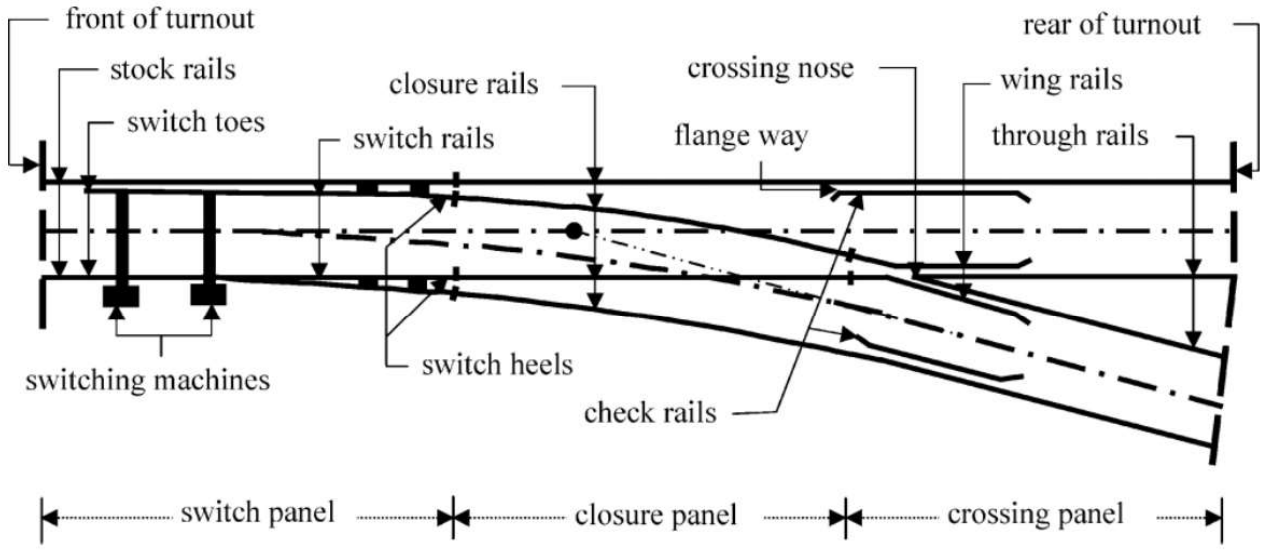


Figure 1.1: *Components of a turnout (from Kassa et al. 2006).*

for traffic both in the straight (through) route and in the branching (diverging) route. Depending on the direction of traffic, either the crossing rail or the wing rail is exposed to the impact. The former is true in the facing move (traffic from switch panel to crossing panel), while the latter holds for traffic in the trailing move (from crossing panel to switch panel). This results in a degradation of the running surface of turnout components over time. An example for the crossing nose can be seen in Figure 1.2.

In 2014, the estimated cost for maintenance of railway turnouts in Sweden was 400 – 450 million SEK, corresponding to around 12% of the overall railway maintenance costs. These costs are, for example, generated because of the needs for repair and replacement of switch rails and crossings due to damage in the forms of wear (i.e. removal of material from the surface), accumulated permanent (plastic) deformation, and breaking out of material caused by surface or subsurface initiated rolling contact fatigue (RCF) cracking, see Figure 1.3.

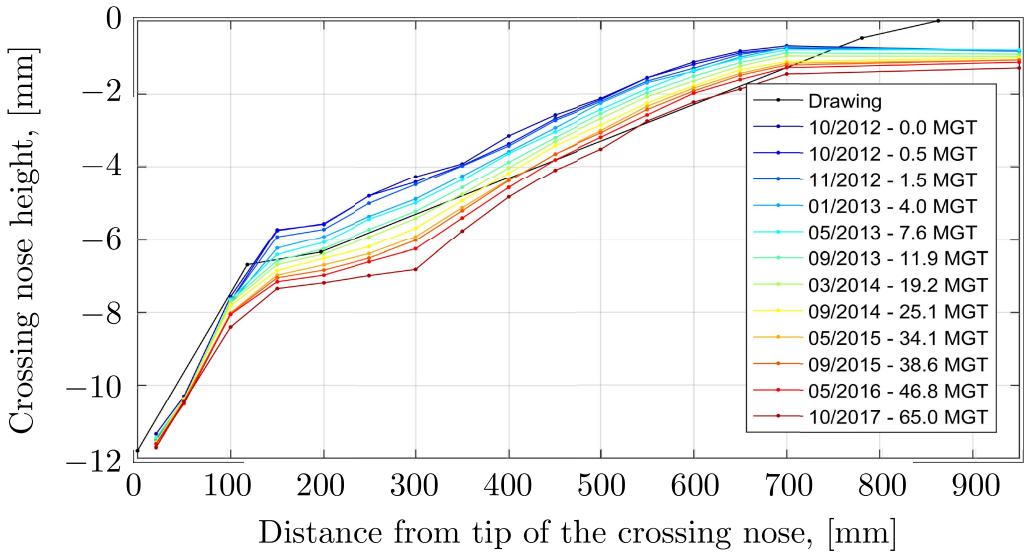


Figure 1.2: *Measured crossing nose height for various amounts of traffic (in MGT). The height has been measured using the top of the wing rail as reference (more details are given in* ***Paper C****).*

(a) *Plastic deformation* (b) *Wear* (c) *Rolling contact fatigue*

Figure 1.3: *Three main damage mechanisms in S&C. Courtesy of voestalpine VAE GmbH.*

## 1.2 Aim of research

For a given traffic situation, the design of an S&C can be adapted to improve performance and reduce maintenance costs. One aspect of this adaption is to select the most suitable crossing material in terms of resistance to long-term damage. In this way, the frequency of maintenance can be reduced. Furthermore, the maintenance activities can be reactive (acting to an existing problem) or preventive (acting shortly before the onset of a problem). The latter type of activity is believed to be financially superior since it provides the benefit of planning and scheduling the activities in advance.

Being able to predict the damage in crossings with reasonable accuracy would aid in a shift towards design optimisation of crossing geometries and materials, and preventive maintenance. The aim of this thesis is therefore to present a simulation methodology to predict and compare the performance of different rail steel grades in terms of long-term plastic deformation and wear in a robust manner. To this end, the following steps have been completed:

- Development of an efficient model for the wheel–rail normal contact accounting for inelastic material response (**Paper A**).
- Design of a load collective that mimics the variability in traffic conditions (**Paper B**).
- Calibration of the material model for the investigated rail steel grades (**Paper B**).
- Demonstration of simulations of plasticity and wear for many load cycles (**Paper B** and **Paper C**).
- Verification of the methodology by comparing simulation results with measurement data from the field (**Paper C**).
- Application of the methodology to a comparison of the long-term damage in turnouts with different crossing angles (**Paper D**).

## 1.3 Scope and limitations

Since the aim of this research has been to carry out simulations of long-term damage in crossings, a large number of load cycles needs to be considered. This comes at a high computational cost. To circumvent this, a number of assumptions and simplifications has been made: 1) the local curvature of wheel and rail around the point of contact is assumed to be constant (same assumption as in the Hertzian theory of contact); 2) multiple simultaneous contact points are assumed to be uncoupled; 3) the wheel is assumed to deform elastically; 4) only the normal contact problem is solved while full slip is assumed for the tangential contact problem; 5) 2D finite element models of cross-sections are used to simulate how plastic deformation evolves during the many load cycles; 6) in each iteration of the methodology (presented in Chapter 8), the simulation of dynamic vehicle–track interaction is carried out assuming a constant rail geometry, which means that the geometry change is not updated after each wheel passage, but after each iteration.

It is assumed that this should suffice for a relative comparison between the performance of different materials. Furthermore, at the time of writing, the available material test data are scarce, especially when it comes to wear, which limits to what extent the damage can be quantified. Lastly, damage attributed to RCF has not been considered in this work.

# 2 Crossing panel design

A wheel travelling over a crossing generally induces an impact load on the crossing rail (in the facing move) or on the wing rail (in the trailing move). The impact load is generated by the downwards-upwards motion experienced by the wheel as it rolls along the wing rail and over to the crossing rail or vice versa, see Figure 2.1. On the wing rail, the vertical motion is caused by the conicity of the wheel and the significant change in lateral wheel–rail contact position that occurs due to the lateral deviation of the wing rail in the running direction. On the crossing rail, the lateral contact position is relatively constant but the crossing rail has a vertical inclination in the running direction.

Increasing vehicle speeds and axle loads, and wheels with severely worn profiles, induce contact conditions that generate higher magnitudes of wheel–rail contact forces and slip. Accelerated rail profile degradation and damage occur if the rail profiles are not corrected in time since deteriorated rail profiles induce contact conditions that further magnify the dynamic loads. As an example, Figure 2.2 (bottom figure) shows a top view of simulated wheel trajectories in the crossing and (top figure) the corresponding normal forces for two vehicles travelling at the same speed and with the same coefficient of wheel–rail friction, but equipped with different wheel profiles. The red lines correspond to wing rail contact, whereas the blue lines denote wheel–rail contact on the crossing nose.

For a given traffic situation, at least three different approaches can be identified as means of reducing the wheel–rail contact forces and damage in the crossing panel by design. These are the optimisations of: 1) crossing and wing rail profiles; 2) stiffness of resilient elements in the crossing, such as rail pads, baseplate pads and implementation of under sleeper pads; and 3) crossing rail material.

The shape of rail profiles along the length of the crossing nose has been optimised in Wan et al. 2014 and in Pålsson 2015. Both studies emphasised that the results of the optimisation were only relevant for the traffic conditions considered. How damage is influenced by crossing angle is quantified in **Paper D**. There, turnouts with three different crossing angles (i.e. curve radii of the diverging route) are compared in terms of long-term plastic deformation and wear.

Based on field measurements in a demonstrator turnout with either soft or medium

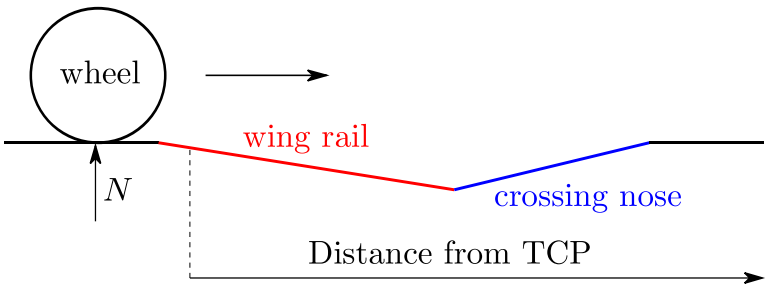


Figure 2.1: *Lateral schematic view of a wheel rolling over a crossing emphasising the vertical movement of the wheel's centre of mass (from **Paper B**).*

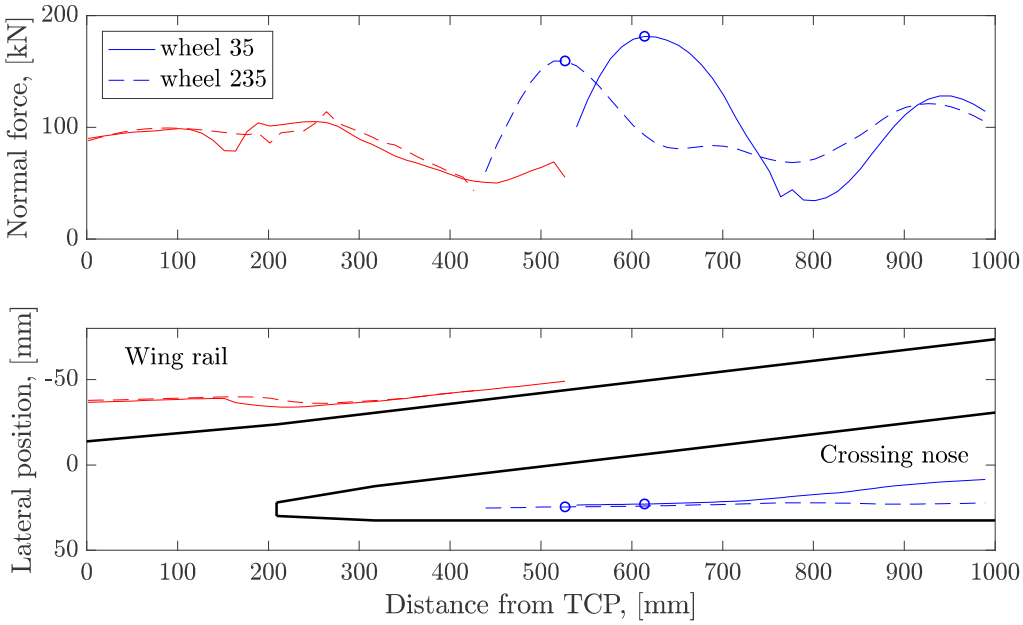


Figure 2.2: *Illustration of wheel transition from wing rail to crossing nose. Normal wheel–rail contact force (top) and top view of contact position (bottom). Maximum normal forces and the corresponding positions on the crossing nose are circled (from* ***Paper D****).*

stiff rail pads, the effect of rail pad stiffness on wheel–rail impact forces was estimated in Pålsson and Nielsen 2015. It was concluded that the impact forces on the crossing can be reduced if softer pads are used. The influence of rail pad stiffness on different damage modes (ballast settlement, wear and RCF of the rails) was evaluated in Grossoni et al. 2016. For the case when the vehicle speed is 40 km/h and support stiffness is 100 MN/m, it was shown that the rail pad properties have little effect on wear, but softer pads aided in RCF damage reduction. However, a more general conclusion was that the rail pad selection should be specific for the line type (stiffer pads should be used for higher speeds). More recently, it was shown in Grossoni et al. 2019 that the variation of support stiffness along the length of a switch panel has little influence on wheel–rail contact forces. In Li et al. 2017, it was demonstrated that the magnitude of the impact load is more influenced by the wheel–rail contact geometry than by the selection of rail pad stiffness. Another study (see Bezin et al. 2020), considered a new conceptual design by elastically mounting a single piece crossing nose on the rest of the casting as means of absorbing impact energy. The stiffness of the proposed resilient crossing nose was considered to be lower than the stiffness of the rail pads. For the studied vehicle speed of 160 km/h, the results showed that the estimated P1 resonance force (due to oscillation of wheel and rail on the wheel–rail contact stiffness, see Jenkins et al. 1974) was reduced by 64% with respect to the reference design, whereas the P2 resonance force (due to oscillation of unsprung vehicle mass and rail on the support stiffness) remained high. The influence of operational parameters was investigated in Ma et al. 2017. It was shown that changes in friction coefficient, wheel acceleration and location of the contact point can cause significant influence on short-term material degradation.

In this thesis, the influence of material selection on long-term rail damage is explored.

Common materials used in crossings include austenitic steels (such as the explosion depth hardened manganese steel Mn13), bainitic steels (B360) and high strength pearlitic rail steels (such as the fine-pearlitic rail grade R350HT). Based on field experience (see e.g. Ossberger et al. 2015), each of these materials has different advantages in terms of resistance to the various types of damage. For example, the manganese steel, which is predominant in the Swedish rail network since the 1990s, has a higher rate of plastic deformation during the initial load cycles but at the same time allows for a better adaptability of rail profile to meet the variation of worn wheel profiles in traffic. A comparison of the short-term performance of crossings made from either rolled Mn13 or R350HT in terms of accumulated plastic deformation and wear after 0.8 million gross tonnes (MGT) of traffic, corresponding to about 3 weeks in operation, is presented in **Paper B**. Since the primary interest of the thesis is the long-term damage in crossings, the amount of simulated traffic was increased to almost 12 MGT in **Paper C**. The predicted plastic deformation and wear were compared to those estimated from in-field crossing measurements, thus serving as a validation of the methodology presented in this thesis.

# 3 Damage in crossings

A review of common damage (material degradation) mechanisms in S&C is given in Dahlberg et al. 2004. The mechanical damage was divided into three categories:

1) Plastic deformation.
2) Wear.
3) Fatigue.

Plastic deformation and wear are the two damage mechanisms considered in this thesis. Figure 3.1 illustrates the measured evolution of a crossing nose rail profile under the combined action of these damage mechanisms.

Plastic (permanent) deformations arise as a result of dislocation movement in grains of the metal due to wheel–rail contact stresses exceeding the yield limit. Plasticity in rail steels can lead to undesirable residual stresses, material hardening and texture (anisotropy) evolution, which impact the initiation and propagation of fatigue cracks.

Wear is the loss of material from a contact surface. In the context of wheel–rail contact, Lewis and Olofsson 2009 identified two situations that induce wear: sliding and rolling. Sliding is more detrimental in terms of wear rate and it is common for wear models to relate the amount of wear to the sliding distance (see e.g. Archard 1953). Even though the rolling motion is mainly associated with the fatigue-driven wear mechanisms, some micro-sliding may occur as well.

Failure of materials due to repeated loading is called fatigue. If the repeated loading cycle does not involve plasticity, the number of cycles before failure will in general be high

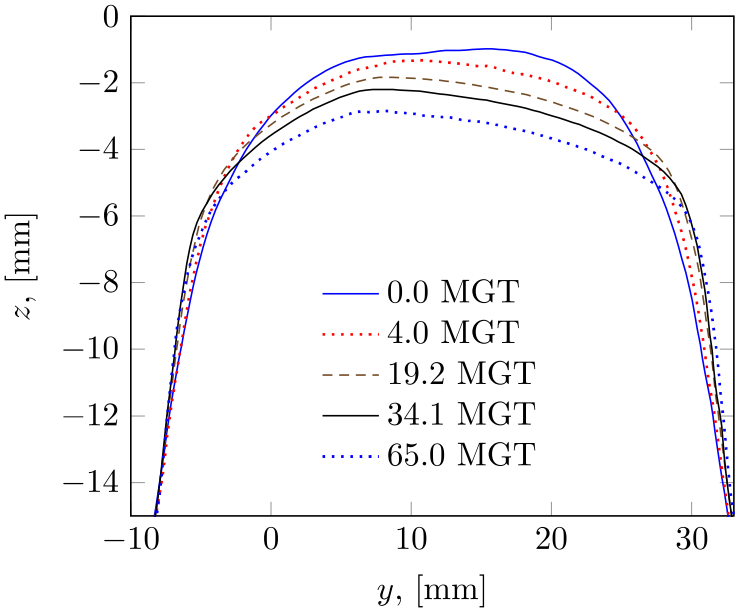


Figure 3.1: *Measured evolution of rail profile vs amount of traffic (in MGT) at cross-section 350 mm after the tip of the crossing (from* ***Paper C****).*

and the process is called high cycle fatigue (HCF). On the other hand, if each loading cycle causes plasticity, the failure usually occurs significantly earlier and this type of fatigue is referred to as low cycle fatigue (LCF). In the context of railways, fatigue is caused by the rolling of the wheel, which is therefore often referred to as rolling contact fatigue (RCF). According to Ekberg and Kabo 2005, some of the distinct features of RCF compared to regular fatigue analysis are:

- Multiaxial stress state at a material point, where the principal stress directions rotate during the load cycle, which complicates quantification of the fatigue life.
- Friction between crack faces due to compressive loading has a considerable effect on the rate of crack growth.

The RCF damage mechanism is usually manifested in the form of either surface or subsurface initiated cracks. Surface initiated RCF cracks stem from plastic deformation of the surface material due to frictional contact (shear stress), which can also result in abrasive wear. The reason for subsurface crack initiation is high compressive contact stress (that peaks some millimetres under the surface) combined with material imperfections. This type of cracks is less common, but more dangerous as it might lead to breaking out of large pieces of the rail material. RCF is tightly connected with the other two damage mechanisms described above. Interestingly, under certain conditions, different damage mechanisms can cancel each other out. This is, for example, true for the case referred to as the Magic Wear Rate (see Magel et al. 2014), when the natural or combination of natural and artificial wear prevents RCF cracks from propagating. For different operating conditions (material properties, track curvature, axle load, vehicle speed, wheel/rail profiles – factors that influence the rates of crack initiation and propagation), it defines the tonnage interval at which the grinding should take place.

# 4 Wheel–rail contact models

One key aspect in the simulation of rail profile degradation is to determine the correct contact stress distribution in the wheel–rail contact. The solution of wheel–rail contact can be divided into two subproblems: normal and tangential contacts. The shape and size of the contact patch are determined by the geometry of bodies, the mechanical response of the materials and the normal force. The influence of the tangential force on the contact pressure is usually small enough for the interaction to be neglected (see Johnson 1987). The resultant stress in the material is obtained by superimposing the effects of the contact pressure and the tangential traction.

## 4.1 Normal contact

Several tools exist for solving the normal contact problem. For example:

1) Hertz theory of contact (Hertz 1881).
2) Kalker's variational method (Kalker 1990).
3) Finite element (FE) method.
4) Metamodel.

The first two approaches are applicable for elastic material response only. In addition, they rely on the assumption that the bodies in contact are large compared with the dimensions of the contact patch, such that they can be considered as infinite half-spaces. The same holds for most fast methods used in vehicle dynamics simulations (see Piotrowski and Chollet 2005): those that replace the contact zone by a set of ellipses and those that are based on virtual penetration of the contacting bodies (or their alternatives that approximate the surface deformation instead of neglecting it, see Sichani et al. 2014a). Furthermore, the theory of Hertz assumes that the geometry of each contact surface can be approximated by an elliptic paraboloid. Kalker's method imposes no restriction on the wheel–rail contact geometry, while the FE simulation approach allows for both arbitrary geometry and inelastic material response. A comparison of the first three approaches within the context of wheel–rail contact can be found in Wiest et al. 2008b. The half-space assumption was inapplicable for the considered cross-section. Nevertheless, the results suggested that both Hertzian and Kalker's solutions correlated well with that of FEM as long as the material response remained elastic. However, it was reported that the maximum contact pressure differed by nearly 60% when plasticity was accounted for, which underlines the importance of considering the elasto-plastic material response.

Typically, the size of the contact patch is in the order of 1 $cm^2$, which is small in comparison with the dimensions of the wheel and rail (see Lewis and Olofsson 2009). Furthermore, the curvatures of wheel and rail contact surfaces can be considered constant over multiple regions of the profiles, see Figure 4.1. However, there are also cases where at least one of the assumptions in Hertzian theory is violated. In particular, such situations

may occur (especially with worn profiles) when the contact is at the gauge corner of the rail or at the flange of the wheel, which might violate the half-space assumption. For such situations, it has been reported by Lewis and Olofsson 2009 that the results of the Hertzian solution are in vast disagreement with FE simulations. In the presence of plastic deformation, the FE method is the only solution that is available, although at a significantly higher computational cost.

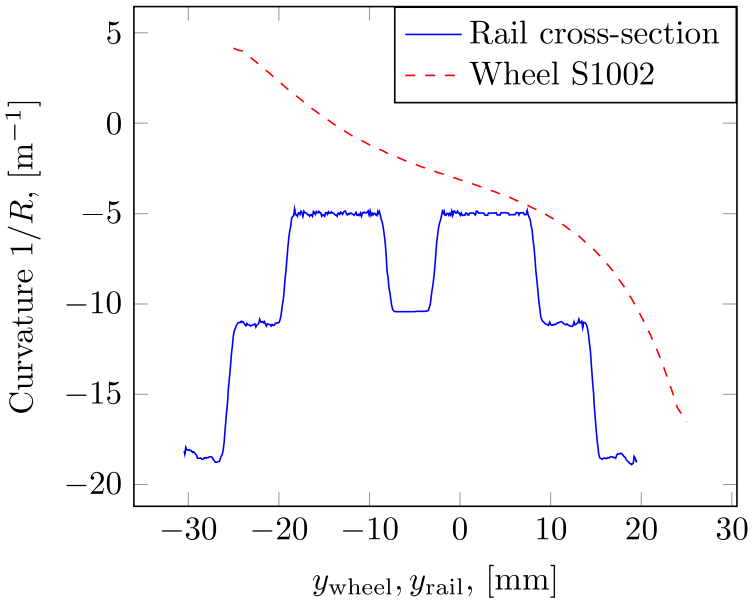


Figure 4.1: *Calculated curvatures within the potential contact area (from **Paper A**). Rail cross-section is located at 1166 mm from the theoretical crossing point in a 60E1-R760-1:15 turnout.*

### 4.1.1 Hertzian solution

The Hertzian solution (see Lundberg and Sjövall 1958) to the normal contact problem is given by two semi-axes $a$ and $b$ of the elliptic contact patch and the pressure distribution $p(x, y)$ within it:

$$a = \left[\frac{3(1-\nu)\alpha^2 F_n E_2}{\pi G \sum \frac{1}{R}}\right]^{1/3} \tag{4.1}$$

$$b = \left[\frac{3(1-\nu) F_n E_2}{\alpha \pi G \sum \frac{1}{R}}\right]^{1/3} \tag{4.2}$$

$$p = p_0 \sqrt{1 - \frac{x^2}{a^2} - \frac{y^2}{b^2}}, \quad |x| \leq a, |y| \leq b, b < a \tag{4.3}$$

where $\dfrac{1-\nu}{G} = \dfrac{1}{2}\left(\dfrac{1-\nu_1}{G_1} + \dfrac{1-\nu_2}{G_2}\right)$ for Poisson's ratios $\nu_{1,2}$ and shear moduli $G_{1,2}$ of the two bodies in contact, $\alpha = a/b$ is the semi-axes ratio, $F_n$ is the normal force, $E_2$ is the

complete elliptic integral of the second kind as a function of the modulus $k = \sqrt{1 - 1/\alpha^2}$, $\sum 1/R$ is the sum of the principal curvatures (each being positive if its centre lies within the body) of the two bodies in contact with angle $\psi$ between the principal planes, and $p_0$ is the maximum contact pressure. These parameters are defined as follows:

$$\sum \frac{1}{R} = \frac{1}{R_x^1} + \frac{1}{R_y^1} + \frac{1}{R_x^2} + \frac{1}{R_y^2} \tag{4.4}$$

$$\alpha = \arg\left(f\left(\alpha; R_x^1, R_y^1, R_x^2, R_y^2\right) = 0\right) \tag{4.5}$$

$$f(\alpha; R_x^1, R_y^1, R_x^2, R_y^2) = g - \frac{(\alpha^2+1)E_2 - 2E_1}{(\alpha^2-1)E_2} \sum \frac{1}{R} \tag{4.6}$$

$$p_0 = \frac{3}{2}\frac{F_n}{\pi ab} \tag{4.7}$$

with $E_1$ being the complete elliptic integral of the first kind (as a function of $k$) and the function $g$ defined as

$$g = \sqrt{\left(\frac{1}{R_x^1} - \frac{1}{R_y^1}\right)^2 + \left(\frac{1}{R_x^2} - \frac{1}{R_y^2}\right)^2 + 2\left(\frac{1}{R_x^1} - \frac{1}{R_y^1}\right)\left(\frac{1}{R_x^2} - \frac{1}{R_y^2}\right)\cos(2\psi)} \tag{4.8}$$

### 4.1.2 Kalker's solution

In Kalker's variational method (see Kalker 1990), the potential contact area is discretised with $N_p$ rectangular elements of size $\Delta x$ by $\Delta y$. For element $I$, a distance $d_I$ between the deformed bodies is introduced as a function of the local vertical displacement $u_{Iz}$, defined as the displacement difference between the two bodies (see Figure 4.2):

$$u_{Iz} = u_{Iz}^1 - u_{Iz}^2 \tag{4.9}$$

The displacement $u_{Iz}$ depends on the pressure $p_{Jz}$ in the contact area and is obtained by summing the individual contributions from each element:

$$u_{Iz} = \sum_{J=1}^{N_p} A_{IzJz} p_{Jz} \tag{4.10}$$

where $A_{IiJj}$ are the influence coefficients. Similarly, the total vertical contact force at the current time step $t_k$ is obtained as

$$F_z(t_k) = \sum_{I=1}^{N_p} p_{Iz} \Delta x \Delta y \tag{4.11}$$

The distance $d_I$, which can be viewed as a kinematic constraint, is defined as

$$d_I = U_z^1 - U_z^2 + u_{Iz} + z_I^1 - z_I^2 + r_I^1 - r_I^2 \tag{4.12}$$

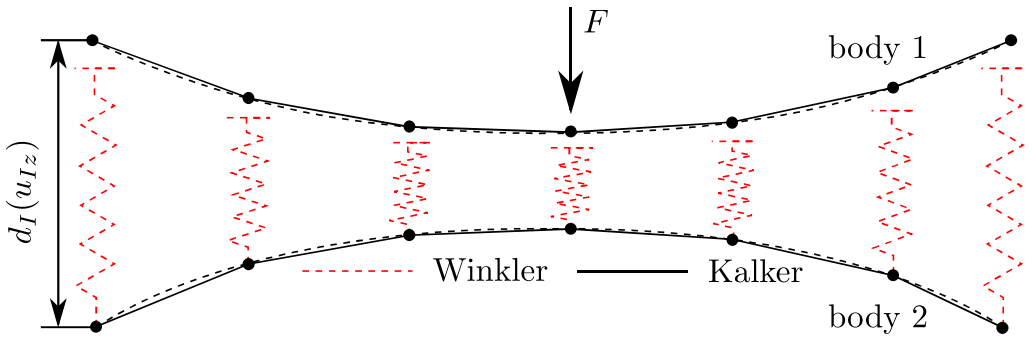


Figure 4.2: *Kalker's and Winkler's models of contact.*

where $U_z^{1,2}$ are global vertical displacements (at time step $t_k$) of the bodies in contact, $z_I^{1,2}$ are the initial vertical coordinates of the element $I$ and $r_I^{1,2}$ are the roughness of the contacting bodies. The contact conditions are as follows:

$$d_I \geq 0, \quad p_{Iz} \geq 0, \quad d_I p_{Iz} = 0 \tag{4.13}$$

The unknown contact force $F_z(t_k)$ is obtained by solving for $p_{Iz}$ the non-linear system of equations 4.10 to 4.13 for given global displacements and roughness. The coefficient $A_{IiJj}$ gives the displacement in the $i$-direction at the centre of element $I$ due to a unit traction in the $j$-direction of element $J$. Kalker's model can be seen as an upgrade of the Winkler bedding model. The spring stiffnesses are replaced with the influence coefficients, and the extended kinematic constraint allows for the coupling of the points of the elastic half-space, which is not present in the Winkler model.

The influence coefficients are used to find the relation between the surface load and the elastic field on the surface and inside the contacting bodies. The half-space is one of the few cases in 3D elasticity for which the influence coefficients are explicitly known. In the general case, these coefficients can only be evaluated numerically by using FEM, although Kalker warns (see Kalker 1990) that they need to be computed with high precision and thus such an approach requires many elements. The influence coefficients of the elements are computed only once for each geometry. Kalker's variational method can also be applied to tangential contact problems. As pointed out in Pieringer 2011, Kalker considered the case where the traction is piecewise constant over the element grid and evaluated the corresponding influence coefficients $A_{IiJj}$. A drawback of this approach can be a high computational cost. This is why many alternative approximate approaches have been devised, e.g. Kalker's FASTSIM algorithm (see Kalker 1982).

### 4.1.3 Finite element solution

A finite element solution of the contact problem is mainly achieved by using one of the two approaches: the penalty method or the Lagrange multipliers method (or its modification the augmented Lagrangian method). The principal difference between the two approaches is in the accuracy of the results. The former method allows the contact surfaces to overlap (which is not physical), whereas the latter one offers an exact alignment of the interfaces

yet at a higher computational cost.

Below follows a brief summary of the main ideas for the case of one deformable body in contact with a rigid surface. Similar, but more complex equations, are valid for two deformable bodies in contact, c.f. Wriggers 2006.

The penalty method introduces a spring with stiffness $\epsilon_N$ at each contact node. This stiffness is referred to as a penalty parameter. The advantage of this method is that the set of unknowns remains unchanged. However, the correct solution is only achieved when $\epsilon_N \to \infty$, but using a too high value leads to an ill-conditioned stiffness matrix. This means the stiffness matrix is almost singular, which leads to large numerical errors when it is inverted. Therefore, the penalty parameter must be limited, which results in a (small) penetration. The system of FE equations to be solved is as follows:

$$\begin{cases} \underline{f}_{\text{int,F}} - \underline{f}_{\text{ext,F}} = \underline{0}, & \text{F} \notin \{s_1, \ldots, s_{n_c}\} \quad (4.14) \\ \underline{f}_{\text{int,F}} - \underline{f}_{\text{ext,F}} + \epsilon_N d(\underline{u}_{\text{F}}) \dfrac{\partial d(\underline{u}_{\text{F}})}{\partial \underline{u}_{\text{F}}} = \underline{0}, & \text{F} \in \{s_1, \ldots, s_{n_c}\} \quad (4.15) \end{cases}$$

where $\underline{f}_{\text{int}}, \underline{f}_{\text{ext}}$ are internal and external force vectors, index F denotes node number with the unknown (not prescribed) displacements $\underline{u}_{\text{F}}$, and $d(\underline{u}_{\text{F}})$ is a gap function (corresponding to $d_I$ in Figure 4.2) obtained from the displacements of the contact nodes $s_i$.

The Lagrange multiplier method introduces additional constraints to the system prescribing that the gap function must be zero for the nodes in contact. It leads to an increase of the number of unknowns. Hence, the absence of penetration of the two bodies comes at a price. The method relies on the following contact conditions (corresponding to 4.13):

$$d \geq 0, \quad \lambda \leq 0, \quad \lambda d = 0 \tag{4.16}$$

i.e. the gap function $d(\underline{u})$ is zero at the point of contact and the additional variable $\lambda$ (called the Lagrange multiplier) is negative. Otherwise, the gap function is positive and the contact force represented by the Lagrange multiplier is zero. If we assume that nodes $s_1$–$s_{n_c}$ are in contact, the equilibrium and contact equations become

$$\begin{cases} \underline{f}_{\text{int,F}} - \underline{f}_{\text{ext,F}} = \underline{0}, & \text{F} \notin \{s_1, \ldots, s_{n_c}\} \quad (4.17) \\ \underline{f}_{\text{int,F}} - \underline{f}_{\text{ext,F}} + \lambda_{\text{F}} \dfrac{\partial d(\underline{u}_{\text{F}})}{\partial \underline{u}_{\text{F}}} = \underline{0}, & \text{F} \in \{s_1, \ldots, s_{n_c}\} \quad (4.18) \\ d(\underline{u}_{\text{F}}) = 0, & \text{F} \in \{s_1, \ldots, s_{n_c}\} \quad (4.19) \end{cases}$$

The advantage of this method is its better precision, since no penetration is allowed. However, the additional degrees of freedom $\lambda_{\text{F}}$ increase the size of the system of equations and, hence, the computational cost.

### 4.1.4 Metamodel

A metamodel (also known as surrogate model) is an approximation model. It is used as a replacement of an actual simulation model typically to reduce the computational

cost. Various metamodelling techniques exist: response surface methodology (Box and Wilson 1951), artificial neural networks (see e.g. Cheng and Titterington 1994), kriging (see e.g. Sacks et al. 1989) to name a few. These techniques usually require a large number of reference data to calibrate the model coefficients. Additionally, the conventional metamodels lack a physical foundation. This is why in the present work, see **Paper A**, it was decided to construct a metamodel based on the Hertzian model for normal contact. It is a non-linear regression model, which allows to account for elasto-plastic material response. The metamodel is given by the following expressions (cf. 4.1-4.7):

$$a = \beta_0 \left[ \frac{\alpha^2 F_n E_2}{\sum \frac{1}{R}} \right]^{\beta_1} \tag{4.20}$$

$$b = \frac{a}{\alpha} \tag{4.21}$$

$$p_0 = \beta_2 \left[ \frac{F_n}{\pi a b} \right]^{\beta_3} \tag{4.22}$$

where $\beta_i$ are model coefficients obtained by calibration against FE results, and the rest of the quantities were defined in Section 4.1.1.

## 4.2 Tangential contact

The tangential part of the contact problem is typically solved using the FASTSIM algorithm (Kalker 1982), which is based on Kalker's simplified theory of rolling contact (Kalker 1973). The simplification is based on the assumption that the surface displacement at a point depends on the traction at that point only, disregarding the contribution of the surrounding points. It was developed to treat elliptic contacts, but can be adapted to non-elliptic problems as well (see e.g. Sichani et al. 2014b for a summary of possible approaches).

During rolling, the distribution of tangential traction $q(x, y)$ within the contact patch is split into two zones (see Figure 4.3): the stick zone where there is no sliding between the contact surfaces, and the slip zone where sliding is present. In the slip zone, the tangential traction reaches its limit value $\mu p(x, y)$ according to Coulomb's law. Here, $\mu$ is the coefficient of friction and $p(x, y)$ is the contact pressure. Kalker combined separate contact conditions for the stick and slip zones into a single one which is satisfied approximately throughout the contact area:

$$|s|\, q + \mu p s = 0, \quad |q| \leq \mu p \tag{4.23}$$

with the (non-dimensional) relative slip $s = (v_1 - v_2)/v$, where $v_1, v_2$ are the velocities of contact particles of the two bodies in contact and $v$ is the rolling velocity.

As summarised in Xu et al. 2017, in FASTSIM the contact patch is discretised into $n_x \times n_y$ rectangular elements of size $\Delta x \times \Delta y$. The relative slip $s(x, y)$ of each element consists of an elastic tangential displacement $u(x, y)$ and a rigid slip $w(x, y)$:

$$s(x, y)\Delta x = u(x, y) - u(x - \Delta x, y) + w(x, y)\Delta x \tag{4.24}$$

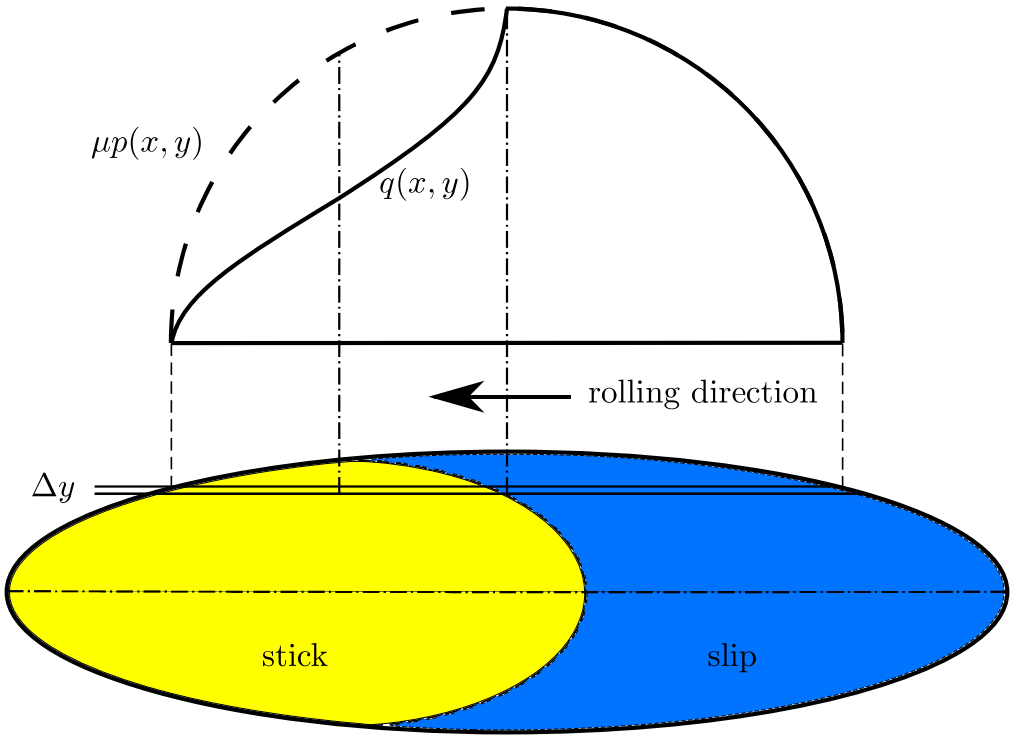


Figure 4.3: *Tractive rolling of an elliptical contact region. Adopted from Johnson 1987.*

with the displacement connected to the shear traction by the flexibility coefficient $L$ (defined in Kalker 1982):

$$u = Lq \tag{4.25}$$

The computation starts at the leading edge of the contact patch, where material points enter the contact zone, and continues in a chain-like fashion, i.e. strip by strip. First it is assumed that no slip occurs, and the trial value of traction $\hat{q}$ yields

$$\hat{q}(x,y) = q(x-\Delta x, y) - w(x,y)\Delta x/L \tag{4.26}$$

If the trial value exceeds the limit value, i.e. $|\hat{q}| > \mu p$, the no-slip assumption was wrong and the value of the tangential traction needs to be corrected:

$$q(x,y) = \mu p(x,y)\frac{\hat{q}(x,y)}{|\hat{q}(x,y)|} \tag{4.27}$$

# 5 Material model

The aim of this thesis is the prediction and comparison of long-term damage in crossings for selected rail steel grades. It is therefore necessary to understand the cyclic behaviour of the materials and be able to model their mechanical response.

One characteristic feature of metals subjected to cyclic loading that involves plastic deformation is ratchetting. Ratchetting is when material accumulates a net strain in the direction of a non-zero mean stress during every cycle. Test data from uniaxial cyclic stress-controlled ratchetting experiments (see Schilke 2013) are used in this study, see **Paper B**. For hot-rolled Mn13 and R350HT, the stress-strain curves for 525 load cycles are shown in Figure 5.1. It is evident that the hot-rolled Mn13 is much softer than R350HT. For example, at 1% strain the stress in Mn13 is half as high as for R350HT. Also, the Mn13 undergoes considerable plastic deformation during the initial cycle. During subsequent cycles, the hot-rolled Mn13 approaches elastic shakedown as the width of the hysteresis loops shrinks and the ratchetting rate slows down. Conversely, R350HT has pronounced ratchetting with a nearly constant shape of the hysteresis loop in each cycle.

A cyclic plasticity model suitable to address ratchetting has been presented in Ohno and Wang 1993. The model assumes linear isotropic elasticity and von Mises yield surface with non-linear kinematic hardening. It is formulated in the small strain framework and the strain is assumed to be additively decomposed into elastic and plastic parts. This model was calibrated against the experiments from Schilke 2013 and is summarised in **Paper B**.

Manganese steel is a common steel grade used in crossings. However, the rolled Mn13

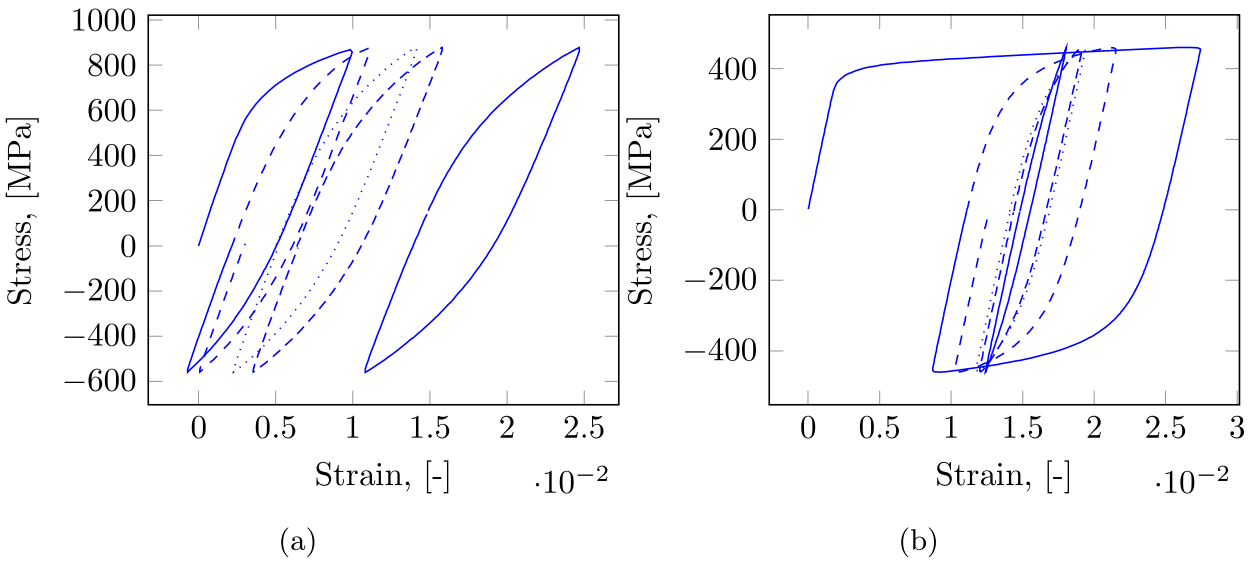


Figure 5.1: *Experiments for 525 load cycles for rail grades (a) R350HT and (b) hot-rolled Mn13 (from **Paper B**). Cycles 1 and 525 are shown as ——, cycle 2 as - - -, cycle 10 as ·····, and cycle 20 as - - - -.*

is too soft and in practice the explosion depth hardened Mn13 is used instead. The explosive hardening process creates a gradient in hardness that is difficult to reproduce in test bars. To mitigate the difference between the excessively soft material, for which the test data are available, and the crossing material, whose deformation was measured in the field, in **Paper C** the yield limit was raised from 351 MPa to 580 MPa (the value provided by crossing manufacturer). In **Paper D**, this high yield limit value was also used in the material model. The wheel was assumed to be linear isotropic elastic in all papers **A**–**D**.

# 6 Simulation of plastic deformation

Laboratory testing of plastic deformation in rails can be traced back to the early 1980s when a two-roller test rig was used to simulate wheel–rail contact on tangent and curved tracks (Kumar et al. 1982). For a standard stock rail material, it was observed that the plastic deformation accumulation stabilised to a constant rate. An attempt to quantify plastic deformation in a numerical simulation followed almost a decade later, see Bower and Johnson 1991. Cyclic strain accumulation was predicted over 100 load cycles showing reasonably good agreement with experimental data from tension-torsion tests, where the specimens were subjected to a load cycle designed to reproduce the stress cycle under sliding contact. A non-linear purely kinematic hardening law for the material was utilised.

Nowadays, non-linear finite element (FE) analysis is the standard tool for the simulation of plasticity in general (no restrictions on geometry) structures. This enables applications of sophisticated material models capable of accurately capturing cyclic plasticity (see e.g. Meyer et al. 2018). An example of application of the FE method to predict cyclic plasticity in turnouts is given in Wiest et al. 2008a. In this reference, the authors investigated how the deformation of the crossing nose due to repeated wheel passages was influenced by the selection of material, although only one wheel profile was used to roll over the same region. Their study suggests that the contact force is gradually reduced for a manganese crossing compared to a tool steel crossing, which is explained by the higher adaptability of the manganese steel. The same conclusion was reached in a recent study (see Wiedorn et al. 2019), which used an FE model of a single wheelset to predict the onset of damage in crossings made of manganese, chromium-bainitic and tool steels. It was also reported that the loading by hollow worn wheel profiles resulted in more plastic deformation and wear than by a new profile.

A method for the assessment of crossing condition was presented in Wei et al. 2018. FE dynamic simulations of plastic deformation and wear were performed based on the measured geometry of a crossing before and after long-term service. The FE model represented a single wheelset with the nominal S1002 wheel profile. The yield limit of the considered damaged rail steel (R260Mn) was estimated via a relation to the measured hardness. A bilinear elastoplastic material model was used for both wheel and rail. A comparison of the simulation results for the initial and long-term serviced geometries showed a widening of the running band as well as an increase of contact patch sizes, which suggested that the crossing experienced the run-in process (adaptation to the load environment) that was also reported in Wiedorn et al. 2018. Consequently, the estimated measures of plastic deformation and wear were lower for the long-serviced geometry, which was reported to be an indication that no urgent maintenance was needed.

The prediction of long-term damage implies that many load cycles need to be simulated. Clearly, this comes at a high computational cost. It is thus desirable to carry out the simulations as numerically efficient as possible. In the procedure described in Johansson and Ekh 2007, an extrapolation technique based on a Taylor series expansion $\varepsilon$ of the material response $\mathcal{S}$ was proposed. The notion *representative time sequence*, illustrated in Figure 6.1, was introduced. The Taylor series of the change in $\mathcal{S}$ from sequence $i$ to

sequence $i + \Delta N$ can be written as

$$\varepsilon_{i+\Delta N} \approx \sum_{n=0}^{m} \frac{\Delta N^n}{n!} D_N^n \mathcal{S}\left(\tau_i\right), \tag{6.1}$$

where $D_N^n$ denotes the $n$th derivative with respect to the sequence number $N$, and $\tau_i$ is the time at the beginning of the $i$th sequence (see Figure 6.1). In practice, a truncation after the second term in the series is applied, see **Paper B**. This extrapolation technique is useful when many load sequences are applied. In **Paper C** and **Paper D**, however, the moderate number of 5 sequences was considered and the extrapolation was not used. In both papers, the predicted plastic deformation was dominating over wear throughout the simulations, although the rate of plastic deformation subsided towards the end.

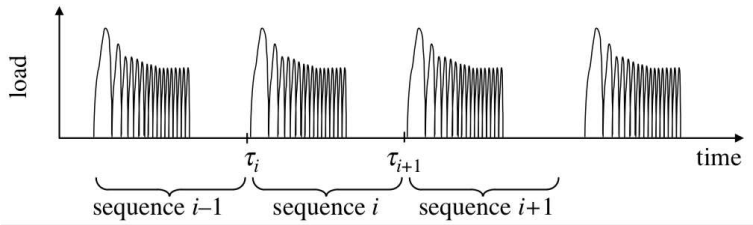


Figure 6.1: *Illustration of representative time sequence exemplified by cyclic loading history (from Johansson and Ekh 2007).*

# 7 Prediction of wear

Two different types of wear models were identified in Enblom 2009. These are (a) models that relate wear to the friction energy dissipated in the wheel–rail contact area, and (b) Archard-based models that attribute wear to the sliding distance, normal force and hardness of the softer material (see Archard 1953). The latter type has attracted a broad field of applications (e.g. it has been used for the prediction of wear in roller bearings, see Olofsson et al. 2000). The wear rate in these types of models depends on the wear regime that can be specified using a wear map, see e.g. Lim and Ashby 1987. However, the generation of a wear map requires extensive testing at different loading conditions and is usually only valid for a given material pair. Due to different wear regimes, wear maps are often discontinuous and a small variation in the contact conditions may lead to an order of magnitude variation in the wear coefficient. Recently, it was shown how a metamodelling technique can be used to construct a continuous wear map, see Cremona et al. 2016.

A comparison of the two types of wear models was performed in De Arizon et al. 2007. The authors compared the Archard-based models used by Jendel 2002, and by Enblom and Berg 2005, with the energy dissipation-based models by Zobory 1997, and Pearce and Sherratt 1991. The models were selected because of their capability of predicting wear in the mild and severe wear regimes and were compared on a theoretical basis. Even though all the models are dependent on experimental coefficients that may not have been estimated in similar test conditions, a reasonable agreement was found. Still, the application of the models to a case of an urban transport vehicle travelling on a network with a distribution of curve radii showed that the model of Pearce and Sherratt predicted wear rates one order of magnitude higher in the severe wear regime than the other models.

Railway turnouts have been identified to be the main driver of wheel wear, see Casanueva et al. 2014. The predicted wheel wear, generated in a turnout without track irregularities, was found to be one order of magnitude higher than the wear on tangent track or curves with irregularities.

Kalker's FASTSIM together with the Archard model have been used to simulate wear in a crossing in papers **B-D**. In **Paper C**, the predicted wear was compared with the estimations from field measurements. The predicted wear rate was nearly constant throughout the simulations, which contradicts the field data. Although the initial wear rate was underestimated by the simulations, the total predicted amount of wear and its distribution after almost 12 MGT of traffic matched rather well.

# 8 Methodology

In Enblom 2009, it was concluded that most studies of wheel/rail damage focus on just one of several damage modes and that models where wear and plastic deformation are integrated are needed. Such a multidisciplinary methodology, allowing to simulate long-term damage in S&C accounting for the variability in traffic conditions, was proposed in Johansson et al. 2011. In this thesis, this methodology is further extended and improved. In each iteration step, the methodology consists of four parts:

I Simulation of dynamic vehicle–track interaction by means of a commercial code (e.g. GENSYS or SIMPACK) in order to predict wheel–rail contact forces, creepages and contact positions. In this thesis, the simulations are carried out in SIMPACK, taking into account stochastic variations of several input parameters, such as vehicle speed and wheel–rail friction (**Paper B**), as well as wheel profiles (papers **B**–**D**).

II Simulation of wheel–rail normal contact using the commercial FE software Abaqus, including a user subroutine UMAT with an elasto-plastic material model to determine realistic contact patches and stresses in the material. Only the rail material is assumed to deform inelastically. To reduce the computational time, local 3D models of the wheel–rail contact are created based on the assumption that the radii of curvature of both wheel and rail are constant in the vicinity of the contact point. In this thesis, to reduce the computational effort, this part of the methodology has been updated with a Hertzian-based metamodel of wheel–rail normal contact (see **Paper A**).

III Simulation of damage evolution. Every load realisation from the simulation of vehicle–track dynamics (part I) and the corresponding contact simulation (part II) constitutes one load cycle. One load sequence is defined by $N$ load cycles, corresponding to $N$ wheel passes. This sequence is repeated $M$ times to obtain the total load collective. This part includes the following damage modes (see **Paper B**):

   a) Plastic deformation. To reduce the computational effort, a plane strain model of the cross-section is used where the normal load is adjusted such that the maximum von Mises stress is identical to the one obtained from the Hertzian-based metamodel in part II.
   b) Wear is calculated using FASTSIM and Archard's wear equation.

IV Profile update. Since the rail profile is not updated after every load cycle, an artifact occurs in the form of an unrealistically deformed cross-section of the rail. In order to alleviate this problem, a smoothing procedure can be applied to the deformed geometry of the rail profile before it is used as input in the next iteration of the methodology. In this thesis, however, no smoothing was used.

Another procedure to predict the life of a turnout based on an explicitly time-integrated FE model has been presented in Xin et al. 2016. It also predicts the elasto-plastic material response assuming non-linear kinematic hardening, but excludes wear. A single wheelset rolling over the crossing is modelled to obtain stresses and strains that are used subsequently in a fatigue model to predict crossing life until crack initiation. Using an FE model, both plastic deformation and wear in a crossing nose were simulated in Wei

et al. 2017. The wheel and rail were modelled assuming bilinear elasto-plastic material behaviour. Wear was accounted for via a frictional work model. The results suggest that the maximum values of both the plastic deformation and wear at the crossing nose occur during the two-point contact stage (during the transition from wing rail to crossing nose) rather than at the instant of maximum normal contact force. In Ma et al. 2018, an explicit FE model of a single wheel with adaptive mesh refinement was used, enhanced with an efficient modelling procedure through the coupling with two-dimensional geometrical contact analysis. The study predicted plastic deformation in a 1:9 crossing panel using a material model with bilinear isotropic hardening. However, unlike in Johansson et al. 2011 and in this thesis, none of these studies took into account the variability in traffic conditions. Also, the cyclic loading was neglected, which may result in an overestimation of rail life.

# 9 Validation

The methodology presented in this thesis has previously been successfully applied to predict the rail profile degradation in a switch panel at Härad in Sweden (see Johansson et al. 2011) and a crossing panel at Haste in Germany (see Nicklisch et al. 2009). In **Paper C**, the methodology is applied to predict the profile evolution of an explosion depth hardened manganese crossing nose in Zeltweg (Austria). The results show good qualitative agreement with measurements after one year of traffic, see Figure 9.1. The three wear peaks observed in the field data, see Figure 9.1(a), are also predicted by the simulations, see Figure 9.1(c). The difference in material properties between the measured and simulated crossings is evident when comparing Figures 9.1(b) and 9.1(d), where rail cross-section shape change is used as a measure of plastic deformation. In the simulations plot, a much larger region is affected by plastic deformation from the start. This indicates that the simulated material response is initially softer than the one estimated from the measurement data. Nevertheless, the long-term simulation results predict the spread of plastic deformation over the length of about 500 mm, which matches the measurement data rather well.

In addition, in **Paper D** the methodology is demonstrated by quantifying the influence of crossing angle on the level of crossing rail degradation. As expected, the results show that a larger crossing angle results in faster profile degradation.

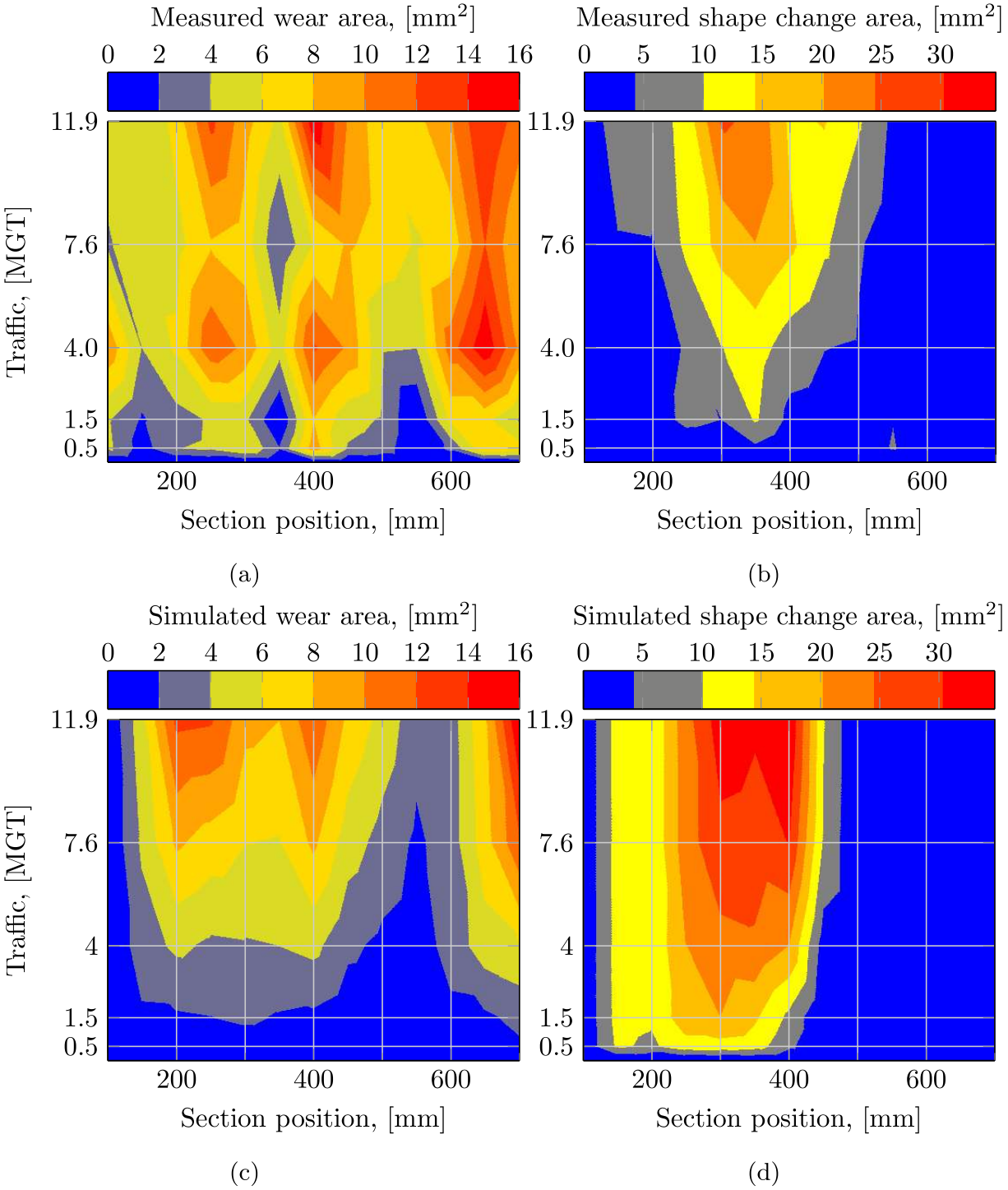


Figure 9.1: *Measurement (a,b) and simulation (c,d) data over time and length of the crossing for different damage measures: (a,c) wear area, [mm$^2$] and (b,d) shape change area, [mm$^2$] (from* ***Paper C****).*

# 10 Summary of appended papers

**Paper A**: **Metamodelling of wheel–rail normal contact in railway crossings with elasto-plastic material behaviour**

Two types of metamodels for the wheel–rail normal contact with elasto-plastic material behaviour are presented. The first one is a linear regression model based on the Response Surface Methodology (see e.g. Myers et al. 2016), while the other one is based on the contact theory of Hertz. Both models approximate the maximum contact pressure and the size of the elliptic contact patch. The inelastic material response is accounted for by calibration against FE simulations with an appropriate material model. An analysis of the performance of the two models shows that the Hertzian-based model is more accurate. The error stemming from the assumption of constant local curvature is quantified. The assumption is concluded to be inadequate for cases with small differences in curvature between the two bodies in contact. However, such cases do not lead to high von Mises stresses and are less detrimental from a material degradation point of view.

**Paper B**: **Prediction of plastic deformation and wear in railway crossings – Comparing the performance of two rail steel grades**

The Hertzian-based metamodel from **Paper A** is incorporated in the simulation methodology, which is applied to compare the short-term performance of two rail steel grades: the fine-pearlitic rail grade R350HT and the austenitic rolled manganese steel Mn13. Plastic deformation and wear are calculated. To account for the spread in traffic conditions, a representative load sequence is generated by means of Latin hypercube sampling. It takes into account variations in worn wheel profile, vehicle speed and wheel–rail friction coefficient. In one iteration of the methodology, 41400 load cycles, corresponding to 0.8 MGT of traffic, were simulated for a selected rail cross-section. The overall change of profile and the amount of ratchetting strain were predicted to be smaller for the crossing made of R350HT, while less accumulated plastic strain was predicted for the rolled Mn13. An adaptive extrapolation algorithm is applied to the plasticity calculations. The wear model is calibrated versus field measurements performed on an explosion depth hardened Mn13 crossing. After 0.8 MGT of traffic, the contribution of wear to the total shape change of the virgin crossing was found to be small, around 2% of the maximum plastic deformation.

**Paper C**: **Long-term profile damage in a railway crossing: Field measurements and numerical simulations**

The simulation methodology is validated versus field measurements for an explosion depth hardened manganese crossing, for which repeated crossing profile measurements are available. The long-term degradation of the crossing was predicted by performing multiple iterations of the simulation methodology corresponding to nearly 12 MGT of traffic (about one year of service time). The influence of the iteration step length and the number of unique wheel profiles on the accuracy of the predicted rail profiles is investigated. The

results suggest that it is acceptable to use relatively large iteration steps, while preserving the accuracy in the long term. However, the number of unique wheel profiles in the load sequence seems to be crucial for the precision of prediction. The simulations predicted a higher rate of damage compared with the one measured in the field. Nevertheless, the methodology showed a good qualitative agreement with measured rail profiles.

**Paper D**: **Influence of crossing angle on long-term damage evolution in railway crossings**

The methodology has been applied for the simulation of plastic deformation and wear in three crossings associated with crossing angles 1:12, 1:14 and 1:18.5. For a given traffic scenario, including up to 52 MGT of facing move passenger traffic in the through route, the results show that the damage increases with increasing crossing angle. The initial high rate of plastic deformation was reduced significantly after the first $2-5$ MGT and after 10 MGT it approached a nearly constant value, whereas the wear rate was nearly constant throughout the simulations. Furthermore, for a given load collective, the results suggest that the rail cross-section with the larger maximum value, but possibly smaller median value, of the resulting maximum von Mises stresses will undergo more plastic deformation.

# 11 Conclusions and future work

> Two roads diverged in a wood, and I –
> I took the one less traveled by,
> And that has made all the difference.
>
> *The road not taken*
> Robert Frost

The current thesis contributes to the development of a simulation methodology for the prediction of long-term degradation of crossing rails in a turnout. The contributions include:

- Development of a Hertzian-based metamodel for wheel-rail normal contact that accounts for elasto-plastic material response. The metamodel was calibrated for two materials: R350HT (**Paper A**) and hot-rolled Mn13 (**Paper B**)
- Calibration of a material model for the prediction of plastic deformation in two rail steels grades: hot-rolled Mn13 and R350HT. The two materials are compared in terms of damage for one cross-section of the crossing rail (**Paper B**)
- Extension of the simulation methodology to multiple iteration steps and to simulation of damage in multiple cross-sections (**Paper C**)
- Validation of the simulation methodology by comparing the predicted long-term damage with field measurement data (**Paper C**)
- Investigation of the importance of selected parameters in the simulation methodology for a robust prediction of long-term damage: number of unique wheel profiles in the load sequence and the frequency of load environment update (**Paper C**)
- Reduction of a vehicle model to a single bogie model while preserving the accuracy of relevant responses (**Paper C**)
- In terms of computational efficiency, improvement of damage calculation by refactoring and parallelising the code (**Paper D**)
- Comparison of simulated long-term crossing rail damage in three turnouts with different crossing angles (**Paper D**)

The presented simulation methodology has been successfully applied to predict long-term crossing rail degradation in terms of plastic deformation and wear. In future work, the methodology may be extended by adding a prediction of crack initiation due to rolling contact fatigue. Also, the possibility of allowing the number of repeated load sequences to vary from one iteration to the next should be investigated. For example, this number could be determined by a maximum allowed change of a profile between two iterations. It is expected that a low number of load sequences is necessary for the initial iterations,

but that higher numbers can be applied after a certain accumulated traffic load when the rate of plastic deformation has been reduced. In principle, after a certain number of iterations, it may even be possible to omit the calculations of plastic deformation if the rate of plastic deformation becomes negligible compared to the wear rate. This would lead to a significant reduction of computational time.

# References


Archard, J. F. (1953). Contact and rubbing of flat surfaces. *Journal of Applied Physics* **24** (8), 981–988. DOI: 10.1063/1.1721448.

Bezin, Y., Kostovasilis, D., and Sambo, B. (2020). Reducing impact loads at railway crossings using tuned resilient elements. *Advances in Dynamics of Vehicles on Roads and Tracks: Proceedings of the 26th Symposium of the International Association of Vehicle System Dynamics, IAVSD 2019, August 12-16, 2019, Gothenburg, Sweden.* Ed. by M. Klomp, F. Bruzelius, J. Nielsen, and A. Hillemyr, pp. 390–396. DOI: 10.1007/978-3-030-38077-9_46.

Bower, A. F. and Johnson, K. L. (1991). Plastic flow and shakedown of the rail surface in repeated wheel–rail contact. *Wear* **144** (1), 1–18. DOI: 10.1016/0043-1648(91)90003-D.

Box, G. E. P. and Wilson, K. B. (1951). On the experimental attainment of optimum conditions. *Journal of the Royal Statistical Society. Series B (Methodological)* **13** (1), 1–45.

Casanueva, C., Doulgerakis, E., Jönsson, P.-A., and Stichel, S. (2014). Influence of switches and crossings on wheel profile evolution in freight vehicles. *Vehicle System Dynamics* **52** (sup1), 317–337. DOI: 10.1080/00423114.2014.898779.

Cheng, B. and Titterington, D. M. (1994). Neural networks: A review from a statistical perspective. *Statistical Science* **9** (1), 2–30. DOI: 10.1214/ss/1177010638.

Cremona, M. A., Liu, B., Hu, Y., Bruni, S., and Lewis, R. (2016). Predicting railway wheel wear under uncertainty of wear coefficient, using universal kriging. *Reliability Engineering & System Safety* **154**, 49–59. DOI: 10.1016/j.ress.2016.05.012.

Dahlberg, T., Ekh, M., Nielsen, J. C. O., and Sällström, J. H. (2004). *State-of-the-art study on railway turnouts: Dynamics and damage.* Research report 2004:8. Department of Applied Mechanics, Chalmers University of Technology, Gothenburg, Sweden, 50 pages.

De Arizon, J., Verlinden, O., and Dehombreux, P. (2007). Prediction of wheel wear in urban railway transport: Comparison of existing models. *Vehicle System Dynamics* **45** (9), 849–866. DOI: 10.1080/00423110601149335.

EC (2011). *White paper: Roadmap to a single European transport area – Towards a competitive and resource efficient transport system.* COM(2011) 144 final. European Commission (EC), 30 pages.

Ekberg, A. and Kabo, E. (2005). Fatigue of railway wheels and rails under rolling contact and thermal loading – An overview. *Wear* **258** (7), 1288–1300. DOI: 10.1016/j.wear.2004.03.039.

Enblom, R. (2009). Deterioration mechanisms in the wheel–rail interface with focus on wear prediction: A literature review. *Vehicle System Dynamics* **47** (6), 661–700. DOI: 10.1080/00423110802331559.

Enblom, R. and Berg, M. (2005). Simulation of railway wheel profile development due to wear – Influence of disc braking and contact environment. *Wear* **258** (7), 1055–1063. DOI: 10.1016/j.wear.2004.03.055.

Grossoni, I., Bezin, Y., and Neves, S. (2016). Optimization of support stiffness at a railway crossing panel. *Proceedings of the second international conference on railway technology: research, development and maintenance (Railways 2016)*. Cagliari (Italy).

Grossoni, I., Le Pen, L. M., Jorge, P., Bezin, Y., Watson, G. V., Kostovasilis, D., and Powrie, W. (2019). The role of stiffness variation in switches and crossings: Comparison of vehicle–track interaction models with field measurements. *Proceedings of the Institution of Mechanical Engineers, Part F: Journal of Rail and Rapid Transit*, 1–14. DOI: 10.1177/0954409719892146.

Hertz, H. R. (1881). Über die Berührung fester elastischer Körper (On the contact of elastic solids). *Journal für die reine und angewandte Mathematik* **92**. (For English translation see *Miscellaneous Papers* by H. Hertz, London: Macmillan (1896) 146-162), 156–171.

Jendel, T. (2002). Prediction of wheel profile wear – Comparisons with field measurements. *Wear* **253** (1), 89–99. DOI: 10.1016/S0043-1648(02)00087-X.

Jenkins, H., Stephenson, J., Clayton, G., Morland, G., and Lyon, D. (1974). The effect of track and vehicle parameters on wheel/rail vertical dynamic forces. *Railway Engineering Journal* **3** (1), 2–16.

Johansson, A., Pålsson, B. A., Ekh, M., Nielsen, J. C. O., Ander, M. K. A., Brouzoulis, J., and Kassa, E. (2011). Simulation of wheel–rail contact and damage in switches & crossings. *Wear* **271** (1–2), 472–481. DOI: 10.1016/j.wear.2010.10.014.

Johansson, G. and Ekh, M. (2007). On the modeling of large ratcheting strains with large time increments. *Engineering Computations* **24** (3), 221–236. DOI: 10.1108/02644400710734945.

Johnson, K. L. (1987). *Contact mechanics*. Cambridge University Press, 468 pages.

Kalker, J. J. (1973). Simplified theory of rolling contact. *Delft Progress Report* **1** (1), 1–10.

Kalker, J. J. (1982). A fast algorithm for the simplified theory of rolling contact. *Vehicle System Dynamics* **11** (1), 1–13. DOI: 10.1080/00423118208968684.

Kalker, J. J. (1990). *Three-dimensional elastic bodies in rolling contact*. Vol. 2. Solid Mechanics and its applications. Dordrecht: Springer Netherlands, 331 p. DOI: 10.1007/978-94-015-7889-9.

Kassa, E., Andersson, C., and Nielsen, J. C. O. (2006). Simulation of dynamic interaction between train and railway turnout. *Vehicle System Dynamics* **44** (3), 247–258. DOI: 10.1080/00423110500233487.

Kumar, S., Aronov, V., Rajkumar, B. R., and Margasahayam, R. (1982). Experimental investigation of plastic flow in rails for a laboratory wheel rail simulation. *Canadian Metallurgical Quarterly* **21** (1), 59–66. DOI: 10.1179/cmq.1982.21.1.59.

Lewis, R. and Olofsson, U. (2009). Basic tribology of the wheel–rail contact. *Wheel–rail interface handbook, Woodhead Publishing Limited, Cambridge*, 34–57.

Li, X., Torstensson, P. T., and Nielsen, J. C. O. (2017). Simulation of vertical dynamic vehicle–track interaction in a railway crossing using Green's functions. *Journal of Sound and Vibration* **410**, 318–329. DOI: 10.1016/j.jsv.2017.08.037.

Lim, S. C. and Ashby, M. F. (1987). Overview no. 55 Wear-Mechanism maps. *Acta Metallurgica* **35** (1), 1–24. DOI: 10.1016/0001-6160(87)90209-4.

Lundberg, G. and Sjövall, H. (1958). *Stress and deformation in elastic contacts*. The Institution of Theory of Elasticity and Strength of Materials, Chalmers University of Technology, Gothenburg, Sweden.

Ma, Y., Markine, V., Mashal, A. A., and Ren, M. (2017). Modelling verification and influence of operational patterns on tribological behaviour of wheel–rail interaction. *Tribology International* **114**, 264–281. DOI: 10.1016/j.triboint.2017.04.038.

Ma, Y., Mashal, A. A., and Markine, V. L. (2018). Modelling and experimental validation of dynamic impact in 1:9 railway crossing panel. *Tribology International* **118**, 208–226. DOI: 10.1016/j.triboint.2017.09.036.

Magel, E., Kalousek, J., and Sroba, P. (2014). Chasing the Magic Wear Rate. *Proceedings of the second international conference on railway technology: research, development and maintenance (Railways 2014), Ajaccio, Corsica, France*.

Meyer, K. A., Ekh, M., and Ahlström, J. (2018). Modeling of kinematic hardening at large biaxial deformations in pearlitic rail steel. *International Journal of Solids and Structures* **130-131**, 122–132. DOI: 10.1016/j.ijsolstr.2017.10.007.

Myers, R. H., Montgomery, D. C., and Anderson-Cook, C. M. (2016). *Response surface methodology: Process and product optimization using designed experiments*. 4th ed. John Wiley & Sons, Hoboken, NJ, 856 p.

Nicklisch, D., Nielsen, J. C. O., Ekh, M., Johansson, A., Pålsson, B. A., Zoll, A., and Reinecke, J. (2009). Simulation of wheel–rail contact and subsequent material degradation in switches & crossings. *Proceedings of the 21st Symposium of the International Association of Vehicle System Dynamics, IAVSD 2009, August 17-21, Stockholm, Sweden*, 1–14 (available on CD).

Ohno, N. and Wang, J.-D. (1993). Kinematic hardening rules with critical state of dynamic recovery, part I: Formulation and basic features for ratchetting behavior. *International Journal of Plasticity* **9** (3), 375–390. DOI: 10.1016/0749-6419(93)90042-O.

Olofsson, U., Andersson, S., and Björklund, S. (2000). Simulation of mild wear in boundary lubricated spherical roller thrust bearings. *Wear* **241** (2), 180–185. DOI: 10.1016/S0043-1648(00)00373-2.

Ossberger, U., Eck, S., and Stocker, E. (2015). Performance of different materials in a frog of a turnout. *Proccedings of the 11th International Heavy Haul Conference*. Perth, Australia, pp. 329–336.

Pålsson, B. A. (2015). Optimisation of railway crossing geometry considering a representative set of wheel profiles. *Vehicle System Dynamics* **53** (2), 274–301. DOI: 10.1080/00423114.2014.998242.

Pålsson, B. A. and Nielsen, J. C. O. (2015). Dynamic vehicle-track interaction in switches and crossings and the influence of rail pad stiffness - Field measurements and validation

of a simulation model. *Vehicle System Dynamics* **53** (6), 734–755. DOI: 10.1080/00423114.2015.1012213.

Pearce, T. G. and Sherratt, N. D. (1991). Prediction of wheel profile wear. *Wear* **144** (1), 343–351. DOI: 10.1016/0043-1648(91)90025-P.

Pieringer, A. (2011). Time-domain modelling of high-frequency wheel/rail interaction. PhD thesis. Department of Civil and Environmental Engineering, Applied Acoustics, Chalmers University of Technology, Gothenburg, Sweden.

Piotrowski, J. and Chollet, H. (2005). Wheel–rail contact models for vehicle system dynamics including multi-point contact. *Vehicle System Dynamics* **43** (6-7), 455–483. DOI: 10.1080/00423110500141144.

Sacks, J., Welch, W. J., Mitchell, T. J., and Wynn, H. P. (1989). Design and analysis of computer experiments. *Statistical Science* **4** (4), 409–423. DOI: 10.1214/ss/1177012413.

Schilke, M. (2013). Degradation of railway rails from a materials point of view. PhD thesis. Department of Materials and Manufacturing Technology, Materials Technology, Chalmers University of Technology, Gothenburg, Sweden.

Sichani, M. S., Enblom, R., and Berg, M. (2014a). A novel method to model wheel–rail normal contact in vehicle dynamics simulation. *Vehicle System Dynamics* **52** (12), 1752–1764. DOI: 10.1080/00423114.2014.961932.

Sichani, M. S., Enblom, R., and Berg, M. (2014b). Comparison of non-elliptic contact models: Towards fast and accurate modelling of wheel–rail contact. *Wear* **314** (1), 111–117. DOI: 10.1016/j.wear.2013.11.047.

Wan, C., Markine, V., and Shevtsov, I. (2014). Improvement of vehicle-turnout interaction by optimising the shape of crossing nose. *Vehicle System Dynamics* **52** (11), 1517–1540. DOI: 10.1080/00423114.2014.944870.

Wei, Z., Núñez, A., Boogaard, A., Dollevoet, R., and Li, Z. (2018). Method for evaluating the performance of railway crossing rails after long-term service. *Tribology International* **123**, 337–348. DOI: 10.1016/j.triboint.2018.03.016.

Wei, Z., Shen, C., Li, Z., and Dollevoet, R. (2017). Wheel–rail impact at crossings: Relating dynamic frictional contact to degradation. *Journal of Computational and Nonlinear Dynamics* **12** (4), 11 pages. DOI: 10.1115/1.4035823.

Wiedorn, J., Daves, W., Ossberger, U., Ossberger, H., and Pletz, M. (2018). Numerical assessment of materials used in railway crossings by predicting damage initiation – Validation and application. *Wear* **414-415**, 136–150. DOI: 10.1016/j.wear.2018.08.011.

Wiedorn, J., Daves, W., Ossberger, U., Ossberger, H., and Pletz, M. (2019). Finite element model for predicting the initiation of subsurface damage in railway crossings—A parametric study. *Proceedings of the Institution of Mechanical Engineers, Part F: Journal of Rail and Rapid Transit* **233** (6), 614–628. DOI: 10.1177/0954409718797039.

Wiest, M., Daves, W., Fischer, F., and Ossberger, H. (2008a). Deformation and damage of a crossing nose due to wheel passages. *Wear* **265** (9), 1431–1438. DOI: 10.1016/j.wear.2008.01.033.

Wiest, M., Kassa, E., Daves, W., Nielsen, J., and Ossberger, H. (2008b). Assessment of methods for calculating contact pressure in wheel-rail/switch contact. *Wear* **265** (9). Contact Mechanics and Wear of Rail/Wheel Systems - CM2006, 1439–1445. DOI: 10.1016/j.wear.2008.02.039.

Wriggers, P. (2006). *Computational contact mechanics.* Springer, 518 p.

Xin, L., Markine, V., and Shevtsov, I. (2016). Numerical procedure for fatigue life prediction for railway turnout crossings using explicit finite element approach. *Wear* **366**, 167–179. DOI: 10.1016/j.wear.2016.04.016.

Xu, J., Wang, P., Ma, X., Xiao, J., and Chen, R. (2017). Comparison of calculation methods for wheel–switch rail normal and tangential contact. *Proceedings of the Institution of Mechanical Engineers, Part F: Journal of Rail and Rapid Transit* **231** (2), 148–161. DOI: 10.1177/0954409715624939.

Zobory, I. (1997). Prediction of wheel/rail profile wear. *Vehicle System Dynamics* **28** (2-3), 221–259. DOI: 10.1080/00423119708969355.

Zwanenburg, W.-J. (2009). Modelling degradation processes of switches & crossings for maintenance & renewal planning on the Swiss railway network, 154. DOI: 10.5075/epfl-thesis-4176.